Field-directed and Template-assisted Magnetic Nanoparticle Self-assembly

Xiaozheng Xue[1] and Edward P. Furlani[1, 2]

1 Dept. of Chemical and Biological Engineering, University at Buffalo SUNY,
Email:xiaozhen@buffalo.edu
2 Dept. of Electrical Engineering, University at Buffalo SUNY,
Office: (716) 645-1194 Fax: (716) 645-3822, Email:efurlani@buffalo.edu

ABSTRACT

A method is presented for controlling the self-assembly of magnetically functional nanoparticles into extended spatial patterns with nanoscale feature resolution. Soft-magnetic template elements embedded in a nonmagnetic substrate are used to guide the assembly. The templates are magnetized using a bias field to produce localized regions of attractive and repulsive magnetic force that enable nanoscale precision of particle placement. The method is demonstrated using a computational model that simulates the assembly process taking into account magnetic and hydrodynamic forces including interparticle interactions, Brownian diffusion, Van der Waals force and effects of surfactants. The analysis shows that complex patterns of particles can be assembled within milliseconds by controlling the particle volume fraction and the core-shell dimensions. The method broadly applies to arbitrary geometries and multi-layer particles having at least one magnetic component. It opens up opportunities for the scalable fabrication of nanostructured materials for a broad range of applications.

Keywords: magnetophoresis, magnetic nanoparticle self-assembly, surfactant-surfactant contact, magnetic dipole-dipole interactions, high-gradient magnetic field, template-based magnetic particle assembly.

1 INTRODUCTION

The interest in non-invasive field-directed control of magnetic particles has grown steadily in recent years due to rapid advances in particle synthesis and related enabling technologies [1-4]. Current applications in this field include drug delivery [5,6], gene transfection [7,8], microfluidic-based bioseparation [9] and sorting [10], and etc. Some emerging applications are focused towards using the directed assembly of magnetic particles to enable a bottom-up approach for the scalable fabrication of nanostructured materials, e.g. for photonic [11,12], magnetic, micro-optical [13] and electronic applications [14,15]. Such an approach would provide advantages over conventional top-down lithographic-based fabrication and would open up opportunities for the low-cost high-throughput production of functional nanostructured materials.

In this presentation we demonstrates a method for controlling the self-assembly of colloidal core-shell nanoparticles into extended spatial patterns with nanoscale resolution. The method holds potential for bottom-up nanoscale fabrication. It involves the use of a uniform bias field combined with localized high-gradient-fields produced by soft-magnetic template elements that are embedded in a nonmagnetic substrate. An example of a system with hollow cylinder template elements is shown in **Fig. 1**. We demonstrate the method using a computational model that simulates the assembly process. The model is based on Langevin's equation and takes into account magnetic and hydrodynamic forces including inter-particle interactions, Brownian diffusion, Van der Waals force and the effects of surfactants. We demonstrate the assembly process for the system shown in **Fig. 1** using core-shell Fe_3O_4-SiO_2 particles. The hollow cylinder template elements produce a force field that focuses the particles into a ring-like pattern. An analytical force expression is used to optimize the dimensions of the elements for this purpose. Once the template element dimensions are known, the computational model is used to simulate the assembly process as a function of the particle volume fraction. The analysis demonstrates that extended particle patterns can be assembled within milliseconds with nanoscale precision. This model can enable the self-assembly of complex patterns of nanoparticles and opens up opportunities for the scalable fabrication of multifunctional nanostructured materials for a broad range of applications.
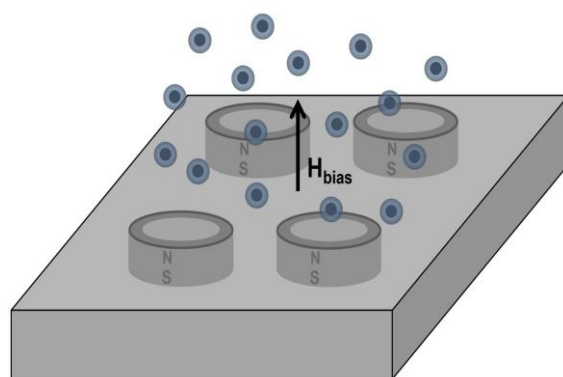

Fig. 1 A self-assembly system showing soft-magnetic hollow cylinder template elements embedded in a nonmagnetic substrate.

2   COMPUTATIONAL MODEL

The behaviour of colloidal magnetic particles in an applied field depends on a number of factors including hydrodynamic and magnetic forces, Brownian motion, Van der Walls force and the effects of surfactants. We predict the self-assembly of such particles using a computational model based on Langevin's equation that takes these effects into account,

$$m_i \frac{d^2 \boldsymbol{x}_i}{dt^2} = \boldsymbol{F}_{mag,i} + \boldsymbol{F}_{vis,i} + \boldsymbol{F}_{B,i}(t)$$
$$+ \sum_{\substack{j=1 \\ j\neq i}}^{N} \left(\boldsymbol{F}_{dd,ij} + \boldsymbol{F}_{vdw,ij} + \boldsymbol{F}_{surf,ij} + \boldsymbol{F}_{hyd,ij} \right), \quad (1)$$

Where m_i and $x_i(t)$ are the mass and position of the i'th particle. The right-hand-side of this equation represents the sum of forces on the i'th particle: $\boldsymbol{F}_{mag,i}$ due to the applied magnetic field, which is a superposition of the bias field and induced gradient-fields; $\boldsymbol{F}_{vis,i}$, viscous drag due to relative motion between the particles and the surrounding fluid (Stokes drag); $\boldsymbol{F}_{B,i}(t)$ a stochastic force to account for Brownian motion; $\boldsymbol{F}_{dd,ij}$ the interparticle magnetic dipole-dipole force due to induced dipole moments; $\boldsymbol{F}_{vdw,ij}$ Van der Waals force; $\boldsymbol{F}_{surf,ij}$ a repulsive force due to surfactant contact between particles and $\boldsymbol{F}_{hyd,ij}$ due to interparticle hydrodynamic interactions. We predict the particle dynamics by numerically integrating Eq.(1) using an adaptive time stepping method to accelerate and stabilize the computation. The various terms in the model and its implementation are briefly described in the following sections.

2.1   Magnetic force

The magnetic force is computed using an "effective" dipole moment method in which the particle is modeled as an "equivalent" point dipole with an effective moment $\boldsymbol{m}_{eff}$. The force on the i'th particle is given by [16]

$$\boldsymbol{F}_{mag,i} = \mu_f \left(\boldsymbol{m}_{i,eff} \cdot \nabla \right) \boldsymbol{H}_a , \quad (2)$$

where μ_f is the permeability of the fluid and H_a is the applied magnetic field intensity at the center of particle. The moment is given by $m_{eff} = V_p M_p$ where $V_p = \frac{4}{3} \pi R_p^3$ and M_p are the volume and magnetization of the magnetic component of the particle, respectively. The moment can be determined using a magnetization model that takes into account self-demagnetization and magnetic saturation of the particles as described in reference [16,17].

2.2   Magnetic dipole-dipole interaction

The potential energy for magnegic dipoles is given by

$$U_{dd,ij} = -\frac{\mu_f}{4\pi} \left(3 \frac{\left(\boldsymbol{m}_{i,eff} \cdot \boldsymbol{r}_{ij} \right)\left(\boldsymbol{m}_{j,eff} \cdot \boldsymbol{r}_{ij} \right)}{r_{ij}^5} - \frac{\boldsymbol{m}_{i,eff} \cdot \boldsymbol{m}_{j,eff}}{r_{ij}^3} \right), \quad (3)$$

where $\boldsymbol{m}_{i,eff}$ and $\boldsymbol{m}_{j,eff}$ are the moments of i'th and j'th particle, respectively, and $\boldsymbol{r}_{ij}$ is the displacement vector between them. The dipole-dipole force in Eq.(1) is obtained as the gradient of the potential,

$$\boldsymbol{F}_{dd,ij} = -\nabla U_{dd,ij} . \quad (4)$$

2.3   Van der Waals interaction

Van der Waals force is given by [18],

$$\boldsymbol{F}_{vdw,ij} = \frac{A}{6} \frac{d_i^6}{(h_{ij}^2 + 2 d_i h_{ij})^2 (h_{ij} + d_i)^3} , \quad (5)$$

where A is the Hamaker constant and h_{ij} is the surface-to-surface separation distance between the i'th and j'th particle.

2.4   Surfactant force

The repulsive force caused by surfactant-surfactant contact is modelled using

$$\boldsymbol{F}_{rep,ij} = -\nabla U_s = \frac{2\pi R_p^2 N_s k_b T}{\delta} \ln(\frac{2R_p + 2\delta}{r_{ij}}) , \quad (6)$$

where R_p, δ and N_s are, respectively, the radius of particle, the thickness of the surfactant layer and the surface density of surfactant molecules [19].

2.5   Viscous drag

The viscous drag on a particle is computed using Stokes' formula

$$\boldsymbol{F}_{D,i} = D \frac{d\boldsymbol{x}_i}{dt} , \quad (7)$$

where $D = 6\pi\eta R_{hyd,p}$ is the drag coefficient, η is the fluid viscosity and $R_{hyd,p}$ is the hydrodynamic radius of the particle.

2.6   Interparticle hydrodynamics interactions

Interparticle hydrodynamic interactions are taken into account using lubrication theory, with a force of the form [18],

$$\boldsymbol{F}_{lub,ij} = \frac{6\pi\mu_f \boldsymbol{V}_{r,i,j}}{h_{ij}} \frac{d_i^2}{16} , \quad (8)$$

where h_{ij} is the separation bewteen the surfaces and $\boldsymbol{V}_{r,i,j}$ is the relative velocity between the particles.

2.7   Brownian diffusion

We impose the following constraint to account for the effetcs of Brownian motion

$$\left\langle x^2 \right\rangle = \frac{2k_B T \Delta t}{D} \qquad \Delta \vec{\boldsymbol{x}}_{B,i} = \vec{\boldsymbol{n}} \cdot \sqrt{\left\langle x^2 \right\rangle} = \vec{\boldsymbol{n}} \cdot \sqrt{\frac{2k_B T \Delta t}{D}} \quad (9)$$

where k_B is Boltzmann's constant, D is the Stokes' drag coefficient as described above, $\Delta \boldsymbol{x}_{B,i}$ is implemented in Eq.(12) and $\vec{\boldsymbol{n}}$ is a randomly generated directional unit vector, which represents the direction of the displacement due to Brownian motion.

2.8   Equations of Motion

Particle motion during assembly is predicted by solving Langevin's equation,

$$m_i \frac{d^2 \boldsymbol{x}_i}{dt^2} + D \frac{d\boldsymbol{x}_i}{dt} = \boldsymbol{F}_{sum,i} + \boldsymbol{F}_{B,i}(t) , \quad (10)$$

where

$$F_{sum,i} = F_{mag,i} + \sum_{\substack{j=1 \\ j \neq i}}^{N} \left(F_{dd,ij} + F_{vdw,ij} + F_{rep,ij} + F_{lub,ij} \right), \qquad (11)$$

Eq. (10) is solved after reduction to coupled first-order system of equations, which are integrated using a numerical time-stepping scheme. The discretized first-order equations are as follows:

$$\Delta x_i = \frac{F_{sum,i}}{D} \tau + \frac{m_i}{D} \left(v_{i,0} - \frac{F_{sum,i}}{D} \right) \left(1 - e^{-\frac{D}{m_i}\tau} \right) + \Delta x_{B,i}, \qquad (12)$$

$$v_{i,f} = \frac{F_{sum,i}}{D} + \left(v_{i,0} - \frac{F_{sum,i}}{D} \right) e^{-\frac{D}{m_i}\tau}, \qquad (13)$$

where τ is the integartion time step, $v_{i,0}$ and $v_{i,f}$ are the velocity of the i'th particle at the beginning and end of the time step and $\Delta x_{B,i}$ is the displacement due to Brownian motion. In our analysis, the time step τ is dynamically adjusted based on the relative velocities and surface-to-surface separations h_{ij} of the particles.

3 RESULTS

We apply the model to study the system shown in **Fig. 1**. Here, the templates are hollow soft-magnetic cylinders that are embedded in a non-magnetic substrate. A uniform bias field H_{bias} is applied perpendicular to the substrate to magnetize the elements. We study the self-assembly of Fe$_3$O$_4$-SiO$_2$ core-shell particles with a core diameter of 30 nm ($R_{core} = 15\ nm$) and a shell thickness of 15 nm. In principle, any multi-layered core-shell particle can be used as long as it has at least one magnetic component. The template elements are permalloy (78% Ni, 22% Fe), which has a saturation magnetization $M_{e,s} = 8.6 \times 10^5\ A/m$. The bias field is taken to be $H_{bias} = 3.9 \times 10^5\ A/m$ ($B_{bias} = 5000\ Gauss$), which is sufficiently strong to saturate both the nanoparticles and the template elements. Their hydrodynamic radius is assumed to be the same as their physical radius $R_{hyd,p} = 60\ nm$. The carrier fluid is assumed to be nonmagnetic with a viscosity and density equal to that of water.

We first analyze the magnetic force. We choose the inner and outer radius and height of the soft-magnetic ring template to be $R_{ring,in} = 400\ nm$, $R_{ring,out} = 500\ nm$ and $h = 200\ nm$, respectively. The spacing between the elements is taken to be 2 μm center-to-center so that there is negligible overlap of their fields. The radial and axial force components $F_{mag,r}$ and $F_{mag,z}$ are computed at a distance $z = 100\ nm$ above the template geometry as shown in **Fig. 2**. Note that there is a relatively strong attractive (downward-directed) axial force $F_{mag,z}$ over the annulus of the element, $R_{in} \leq r \leq R_{out}$ which promotes assembly in this region. Significantly, there is also a relatively weak repulsive (upward-directed) axial force above a substantial portion of its interior region ($0 \leq r \leq R_{in}$), which prevents particles from assembling there. The radial field component $F_{mag,r}$ also plays a critical role in focusing the particles over the

annulus. Note from **Fig. 2a** that it is directed outward over the interior of the annulus $0 \leq r \leq R_{in}$, and inward over the exterior of the annulus $r \geq R_{out}$. Thus, the magnetic force field directs the particles over the annulus, which promotes assembly of the ring structure. It is important to note that the ability to produce regions of attractive and repulsive magnetic force is a key feature of the proposed assembly method as it enables nanoscale precision of particle placement.

Fig. 2 Axisymmetric magnetic force components at $z = 100\ nm$ above the template element: (a) $F_{mag,r}$ and (b) $F_{mag,z}$.

Next, we use the computational model to study the dynamics of the assembly process. The bias field and template dimensions are as above. We use a computational domain centered with respect to a single element. The domain spans a unit cell, i.e. 2 μm along both the x and y axes and 1 μm in the z-direction as shown in **Figs. 3a** and **4a**. The base of the domain is at $z = 0$, which coincides with the top surface of both the substrate and the template element. Periodic boundary conditions for particle transport are imposed at the lateral sides of the domain to account for a 2D array of template elements. We simulate the assembly of 60 nm Fe$_3$O$_4$-SiO$_2$ particles for a range of different percent volume fractions: $\phi = 0.0655, 0.0873, 0.11, 0.131, 0.153$ and 0.175%. These values correlate to an integer number of particles in the computational domain, e.g. $\phi = 0.0655$ and 0.175% correspond to 15 and 40 particles, respectively. The modeling shows that the final assembly for
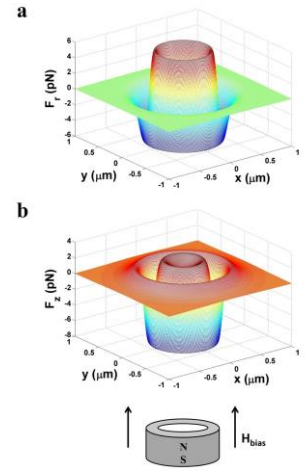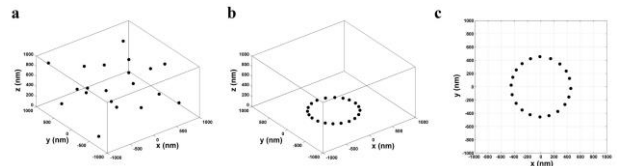

Fig. 3 Initial and final particle distributions for $\phi = 0.0873\%$: (a) initial random particle distribution, (b) perspective of final assembled particle ring, (c) top view of assembled particle ring.
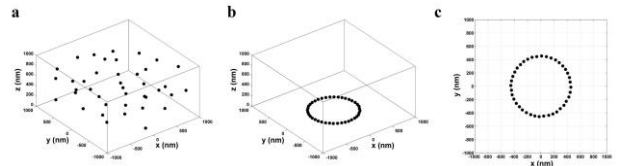

Fig. 4 Initial and final particle distributions for $\phi = 0.1750\%$: (a) initial random particle distribution, (b) perspective of final assembled particle ring, (c) top view of assembled particle ring.

all of the ϕ values is chain-like ring pattern. Representative plots of the initial and final particle distributions for $\phi =$ 0.0873 and 0.1750% are shown in **Figs. 3** and **4**, respectively. In this analysis the particles are initially randomly distributed and their final configuration is a single particle ring pattern that forms over the annulus of the template element. The assembly was completed in less than 30 *ms* for all the cases studied. The final particle assembly has many important features. For example, it has a line width of 60 *nm*, i.e. the diameter of the nanoparticles. This is smaller than the line width of the template element, i.e. the width of the annulus which is 100 *nm*. Another interesting feature is that the particles are nearly uniformly spaced. This occurs because neighboring particles are pushed apart by a mutually repulsive dipole-dipole force, which is due to the alignment of all dipole moments upward, parallel to the applied field.

4 CONCLUSIONS

We have presented a method for directing the assembly of colloidal magnetic-dielectric core-shell nanoparticles into extended geometric patterns with nanoscale precision. Soft-magnetic template elements guide the assembly in the presence of a uniform bias field. The combination of a uniform field and localized gradient fields produced by the template elements enables nanoscale precision of particle placement. We demonstrate proof-of-principle using a computational model that takes into account dominant mechanisms that govern the assembly dynamics. The analysis shows that prescribed geometric patterns of particles can be assembled within milliseconds and with a line width resolution substantially greater than that of the template geometry. The increased resolution is achieved by tailoring parameters that include the template geometry to produce an appropriate force; the thickness of the particle shell to control the magnetic dipole-dipole force and the particle volume fraction to suppress undesired aggregation during assembly. The method broadly applies to arbitrary template geometries and multi-layered particles with at least one magnetic component. Once particle patterns have been formed, they can be transferred to a different substrate using techniques similar to those described by Henderson et al [20]. Thus, a single template substrate can be used to reproduce numerous nano-patterned materials. The ability to produce such materials opens up opportunities for the scalable high-throughput fabrication of multifunctional nanostructured materials for a broad range of applications and our computational model enables the rational design of such media.

ACKNOWLEDGEMENTS

REFERENCES

[1] Pankhurst, Q.A.; Thanh, N.K.T.; Jones, S.K.; Dobson, J. Progress in applications of magnetic nanoparticles in biomedicine. In J. Phys. D Appl. Phys., 2009, 42(22), 224001/224001-224001/224015.

[2] Berry, C.C. Progress in functionalization of magnetic nanoparticles for applications in biomedicine. In J. Phys. D Appl. Phys., 2009, 42(22), 224003/224001-224003/224009.

[3] Pamme, N. Magnetism and microfluidics. In Lab Chip, 2006, 6(1), 24-38.

[4] Furlani, E.P. Magnetic biotransport: analysis and applications. In Materials, 2010, 3, 2412-2446.

[5] Arruebo, M; Fernández-Pacheco, R; Ibarra, M.R; Santamaría, J. Magnetic nanoparticles for drug delivery. In Nanotoday, 2007, 2(3):22–32.

[6] Furlani, E.P.; Xue, X. A Model for Predicting Field-Directed Particle Transport in the Magnetofection Process. In Pharm. Res., 2012, 29(5), 1366-1379.

[7] Dobson, J. Gene therapy progress and prospects: magnetic nanoparticle-based gene delivery. In Gene Ther., 2006, 13(4), 283-287.

[8] Furlani, E.P.; Xue, X. Field, force and transport analysis for magnetic particle-based gene delivery. In Microfluid. Nanofluid., 2012, 13(4), 589-602.

[9] Ganguly, R.; Puri, I.K. Microfluidic transport in magnetic MEMS and bioMEMS. In Wiley Interdiscip. Rev. Nanomed. Nanobiotechnol., 2010, 2(4), 382-399.

[10] Zborowski, M; Chalmers J.J. Magnetic cell separation, vol 32 (Laboratory techniques in biochemistry and molecular biology). In Elsevier Science, 2007, New York.

[11] Xia, Y.; Gates, B.; Li, Z.-Y. Self-assembly approaches to three-dimensional photonic crystals. In Adv. Mater. (Weinheim, Ger.), 2001, 13(6), 409-413.

[12] Yethiraj, A.; Thijssen, J.H.J.; Wouterse, A.; Van Blaaderen, A. Large-area electric-field-induced colloidal single crystals for photonic applications. In Adv. Mater. (Weinheim, Ger.), 2004, 16(7), 596-600.

[13] Lu, Y.; Yin, Y.; Xia, Y. A self-assembly approach to the fabrication of patterned, two-dimensional arrays of microlenses of organic polymers. In Adv. Mater. (Weinheim, Ger.), 2001, 13(1), 34-37.

[14] Hochbaum, A.I.; Fan, R.; He, R.; Yang, P. Controlled growth of Si nanowire arrays for device integration. In Nano Lett., 2005, 5(3), 457-460.

[15] Shipway, A.N.; Katz, E.; Willner, I. Nanoparticle arrays on surfaces for electronic, optical, and sensor applications. In ChemPhysChem, 2000, 1(1), 18-52.

[16] Furlani, E.P. Analysis of particle transport in a magnetophoretic microsystem. In J. Appl. Phys., 2006, 99(2), 024912/024911-024912/024911.

[17] Furlani, E.P.; Ng, K.C. Nanoscale magnetic biotransport with application to magnetofection. In Phys. Rev. E Stat., Nonlinear, Soft Matter Phys., 2008, 77(6-1), 061914/061911-061914/061918.

[18] Russel, W.B.; Saville, D.A.; Schowalter, W.R., Colloidal Dispersions, Cambridge University Press, 1989.

[19] Rosensweig, R.E. Fluid dynamics and science of magnetic liquids. In Advances in Electronics and Electron Physics. 1979, Vol. 48: Martin M (ed.) Academic Press, New York, pp. 103-99.

[20] Henderson, J.; Shi, S.; Cakmaktepe, S.; Crawford, T.M. Pattern transfer nanomanufacturing using magnetic recording for programmed nanoparticle assembly. In Nanotechnology, 2012, 23(18), 185304/185301-185304/185308.